Impact of X-ray Scatter When Using CT-based Attenuation Correction in PET: A Monte Carlo Investigation

Habib Zaidi, *Senior Member, IEEE and* Mohammad Reza Ay, *Member, IEEE*

***Abstract*— Current dual-modality PET/CT systems offer significant advantages over stand-alone PET including decreased overall scanning time and increased accuracy in lesion localization and detectability. However, the contamination of 3-D cone-beam CT data with scattered radiation during CT-based attenuation correction (CTAC) is known to generate artifacts in the attenuation map and thus the resulting PET images. The aim of this work is to quantitatively measure the impact of x-ray scatter in CT images on the accuracy of CTAC on future designs of volumetric PET/CT systems. Our recently developed MCNP4C-based Monte Carlo x-ray CT simulator capable of modeling both fan- and cone-beam CT scanners and the *Eidolon* dedicated 3D PET Monte Carlo simulator were used to generate realigned PET/CT data sets. The impact of x-ray scatter was investigated through simulation of a uniform cylindrical water phantom for both a commercial multi-slice and prototype flat panel detector-based cone-beam CT scanners. The analysis of attenuation correction factors (ACFs) for the simulated cylindrical water phantom showed that the contamination of CT data with scattered radiation in the absence of scatter removal underestimates the true ACFs, namely by 7.3% and 28.2% in the centre for both geometries, respectively. It was concluded that without appropriate x-ray scatter compensation, the visual artifacts and quantitative errors in flat panel detector-based geometry are substantial and propagate cupping artifacts to PET images during CTAC.**

I. Introduction

Quantitative image reconstruction in PET requires an accurate attenuation map (μmap) of the object under study for the purpose of attenuation correction. Several investigators tried to characterize quantitatively the effect of physical and physiological factors on the accuracy of CT-based attenuation correction (CTAC) in PET. In particular, the contamination of CT data with scattered radiation, which depends on the geometry of the CT scanner and object under study, reduces reconstructed CT numbers and introduces cupping artefacts in the reconstructed images [1]. This effect is more pronounced in the next generation of CT scanners with flat panel detector-based cone-beam configurations, which are much less immune to scatter than fan-beam CT scanners [2]. The magnitude and spatial distribution of scattered radiation in x-ray CT for both fan- and cone-beam geometries should be accurately quantified for optimization of scanner design geometry and development of robust scatter correction techniques. This problem has been historically addressed by different groups in the context of using CT for quantitative measurements by means of experimental studies, mathematical modeling and Monte Carlo simulations for both fan- and cone-beam geometries [2]. It should be noted that most published papers assessing the distribution of scattered radiation in the fan-beam geometry used either straightforward experimental measurements or in-house developed Monte Carlo simulators modeling old CT scanner technologies based on gaseous (Xenon) detectors, whereas the characterization of scattered radiation in current generation CT scanners with accurate modeling of single- and multi-row scintillation detector technology has been addressed recently by our group [3]. In addition, to the best of our knowledge, the assessment of the impact of scatter in CT images on the accuracy of CT-based attenuation correction has never been addressed before, neither in the fan-beam geometry with multi-row detector configuration nor in the cone-beam geometry with flat panel detectors. The aim of this study is to investigate the impact of x-ray scatter in CT images on the accuracy of CTAC using dedicated x-ray CT [3] and 3D PET [4] Monte Carlo simulations. Both commercially available fan-beam multi-slice and future generation cone-beam flat panel detector-based CT scanners were considered. For the latter, a hypothetical cone-beam CT mimicking the geometry of a prototype flat panel detector-based CT scanner [5] adjusted to the dimensions of large area panel PET detectors under development by CPS Innovations (Knoxville, TN) [6] for next generation PET/CT systems was simulated.

II. Materials and Methods

A. Monte Carlo Simulation

The MCNP4C-based Monte Carlo x-ray CT simulator [3] was used for simulation of LightSpeed four-slice CT scanner (GE Healthcare Technologies, Waukesha, WI) and cone-beam

This work was supported by the Swiss National Science Foundation under grant SNSF 3152A0-102143.

Habib Zaidi is with the Division of Nuclear Medicine, Geneva University Hospital, CH-1211 Geneva, Switzerland (e-mail: habib.zaidi@hcuge.ch).

Mohammad Reza Ay was with the Division of Nuclear Medicine, Geneva University Hospital, CH-1211 Geneva, Switzerland. He is now with the Department of Medical Physics, Tehran University of Medical Sciences, Tehran, Iran (e-mail: mohammadreza_ay@tums.ac.ir).

1-4244-0561-0/06/$20.00 ©2006 IEEE.

panel detector-based CT scanner based on the geometry of a prototype flat panel detector-based CT scanner [5] modified to fit the size of LSO detector modules proposed for a panel-based PET scanner [6] for similar axial coverage. Full simulation of x-ray spectra including tracking the electrons into the x-ray tube target for the calculation of bremsstrahlung and produced characteristic photons was considered [7]. The collimator inside the detector housing (septa) in the LightSpeed scanner was accurately modelled through full photons transport inside the septa plates. After simulation of all views, a filtered backprojection reconstruction algorithm was used for image reconstruction of the simulated data sets. Likewise, the *Eidolon* 3D PET Monte Carlo simulator [4] was used to acquire emission data corresponding to the geometry of the ECAT ART PET scanner (CTI/Siemens, Knoxville, TN). Experimental and/or clinical validation of the PET and CT simulators is described elsewhere [3,4,8].

B. Attenuation Correction and Image Reconstruction

The computation of ACFs derived from CTAC involved down-sampling the CT image matrix to 128×128 followed by Gaussian smoothing using a 6 mm kernel to match the spatial resolution of the PET scanner used in this study. CT numbers (in HU) were then transformed to linear attenuation coefficients at 511 keV using the calculated bi-linear curve. The created μmaps were forward projected to generate 47 ACF sinograms. The attenuation corrected projections were reconstructed using the 3DRP reprojection algorithm implemented within the ECAT 7.2.1 software (CTI Molecular Imaging Inc., Knoxville, TN) with a maximum acceptance angle corresponding to 17 rings and a span of 7. The default parameters used in clinical routine were applied (Ramp filter, cut-off frequency 0.35 cycles/pixel). The reconstructed images consist of 47 slices with 128×128 resolution and a voxel size set to $1.72\times1.72\times3.4$ mm^3.

C. Scattered Radiation Modeling

To evaluate the impact of scattered radiation on CT images during CTAC in both fan-beam multi-slice and cone-beam panel detector-based CT, a cylindrical water phantom (200 mm diameter) was simulated for both geometries. Likewise, PET data of the same phantom with uniformly distributed activity of ^{18}F were simulated using *Eidolon*. The scatter contribution during the simulation of CT data was separated from the primary component using the surface source method implemented in the MCNP4C Monte Carlo code. In this method, a virtual plane is considered after the scatter medium (water phantom) and the direction, energy and history of each photon passing through this plane is registered. In the next step, the scatter component is calculated by considering only photons which had at least one interaction before hitting this plan toward the detection system. The unscattered component is calculated using the same method by considering only photons which had no interaction before hitting the virtual plane. The beam hardening effect was removed from the projections according to the method described by Kanamori *et al.* [9] to isolate its effects from scatter. The accuracy of beam hardening removal was validated by comparing corrected profiles with those simulated using monoenergetic photons with the effective CT energy (72 keV for the LightSpeed CT scanner operated at 120 kVp). The latter was calculated using experimental measurements based on the method proposed by Bai *et al.* [10]. Scatter correction of the simulated CT data was not performed for both fan- and cone-beam geometries to allow the assessment of the impact of x-ray scatter on the accuracy of CTAC in the absence of antiscatter grids and robust scatter correction algorithms. However, the physical scatter rejection components (septa) always present in multi-slice CT scanners were accurately modelled during the simulation. Thereafter, the simulated primary and total (sum of primary and scattered photons) projections were reconstructed using a filtered backprojection algorithm.

To assess the differences between the energy-dependent scatter components when using x-ray CT and radionuclide-based transmission scanning at 511 keV (e.g. ^{68}Ga/^{68}Ge), the μmap was generated for both conditions, i.e. using the x-ray spectra and mono-energetic 511 keV photons as input to the Monte Carlo CT simulator. To avoid the effect of using different imaging geometries and source configurations, the projections were simulated for both energies using the same scanner (LightSpeed CT scanner).

III. RESULTS

Fig. 1 shows Monte Carlo simulated scatter profiles for the cylindrical water phantom (200 mm diameter) calculated for CT (x-ray spectra, 120 kVp) and monoenergetic PET (511 keV) energies.

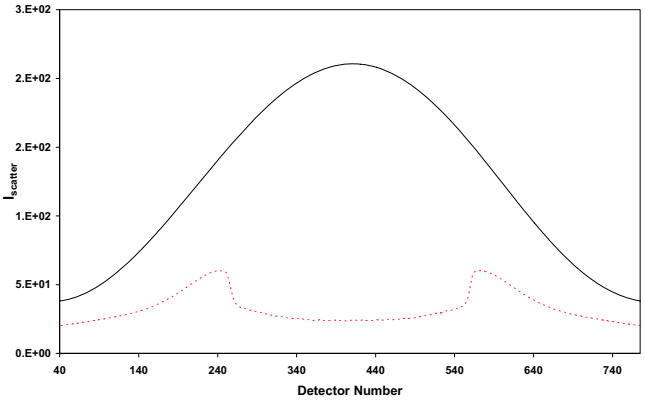

Fig. 1. Simulated scatter profiles for a cylindrical water phantom (200 mm diameter) in both 120 kVp x-ray spectra (doted line) and monoenergetic 511 keV photons (solid line) using a dedicated Monte Carlo x-ray CT simulator.

A total number of 1.9×10^9 photons were simulated. The fan-beam angle was adjusted to cover the water phantom in order to increase the simulation efficiency. The magnitude and

spatial distribution of the scatter component for the x-ray spectra is quite different from the scatter component at 511 keV owing to the difference in terms of dominations by photoelectric and Compton interactions occurring in different energy ranges, which might preclude application of scatter correction algorithms developed for radionuclide transmission scanning to CT data even with appropriate rescaling [11].

The comparison of simulated attenuation profiles for primary and total projection data of the cylindrical water phantom in both fan- and cone-beam CT geometries is shown in Fig. 2a. It should be noted that the total profile for the cone-beam CT was taken from the central elements of the flat panel detector for comparison with the fan-beam geometry. The maximum value for primary and total fan- and cone-beam profiles is 4.26, 4.13 and 3.61, respectively. The underestimation of attenuation profiles for the cone-beam geometry is the consequence of substantial contribution of scattered radiation. The central profile of the corresponding reconstructed CT images is shown in Fig. 2b. The typical cupping artifact apparent on the reconstructed images for the cone-beam geometry illustrates the important influence of scattered radiation on the quality of reconstructed CT images. It should be noted that the effect of beam hardening was removed from the profiles before reconstruction. The central profile of the corresponding CTAC-based μmap of the cylindrical water phantom at monoenergetic 511 keV photons is shown in Fig. 2c. The calculated linear attenuation coefficient in the central region of μmaps created from the primary, total fan-beam and cone-beam CT images is 0.0958, 0.0926 and 0.0782 cm^{-1}, respectively. The latter value deviates considerably from the theoretical linear attenuation coefficient in water at 511 keV (0.096 cm^{-1}). Fig. 2d compares central profiles of ACFs computed using calculated AC (CAC) based on the theoretical value of the linear attenuation coefficient of 511 keV photons in water and the generated μmaps using CTAC. The maximum ACF in the central part is 7.73, 7.64, 7.18 and 5.55 when using CAC and CTAC primary, total fan-beam and total cone-beam, respectively. This reveals that the contamination of CT data with scattered radiation in the absence of scatter removal underestimates the true ACFs in the

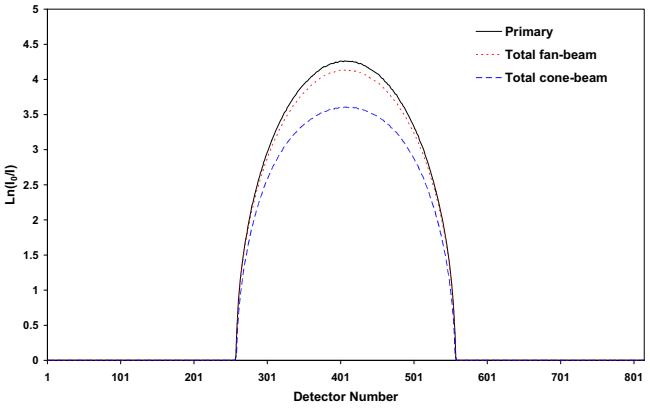

(a)

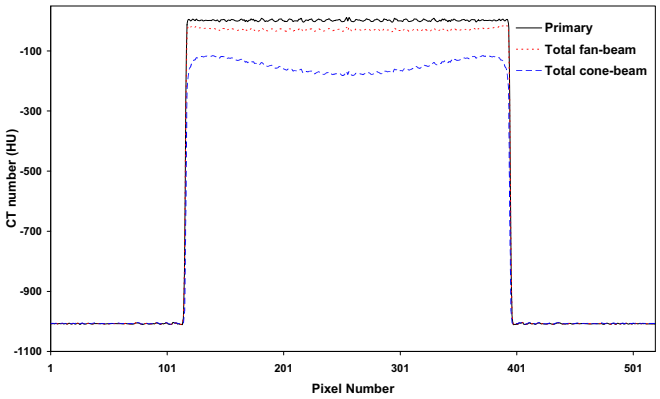

(b)

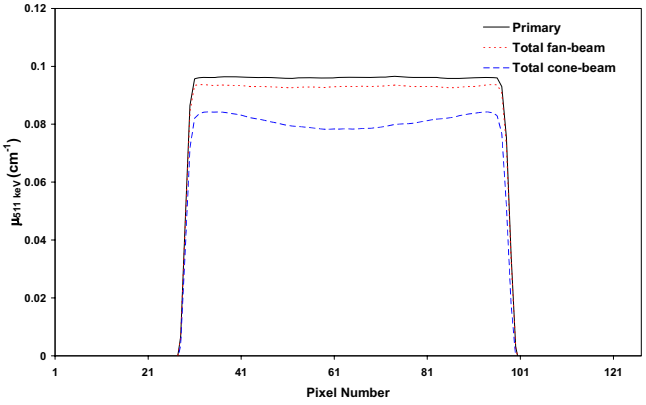

(c)

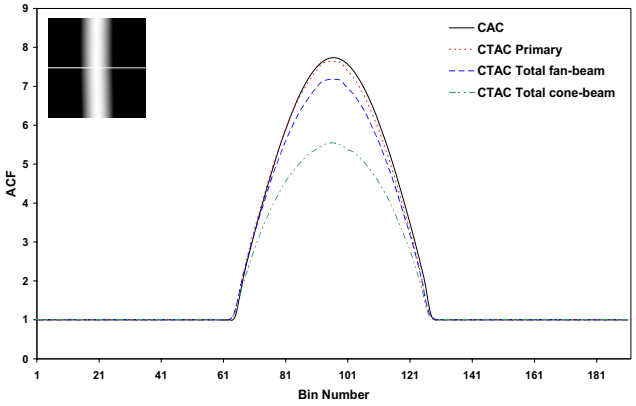

(d)

Fig. 2. Monte Carlo simulations of the cylindrical water phantom (200 mm diameter) in both fan- and cone-beam CT geometries showing: (a) attenuation profiles of primary and total events; (b) central profiles through reconstructed CT images; (c) central profiles through μmaps at 511 keV generated using the bi-linear transformation method; and (d) central profiles through ACF sinograms calculated from μmaps shown in (c).

centre of the cylindrical phantom by 7.3% and 28.2% for fan-beam and total cone-beam geometries, respectively.

The reconstructed images after attenuation correction of simulated emission data using the ACF sinograms calculated with different methods are shown in Fig. 3a. Fig. 3b shows central profiles of activity concentration from the reconstructed images. The average relative difference between

the profiles drawn on images reconstructed using the different methods for deriving the CT-based attenuation map and CAC serving as gold standard is 1.58%, 7.98% and 30.18%, respectively.

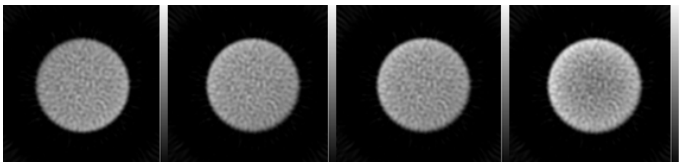

(a)

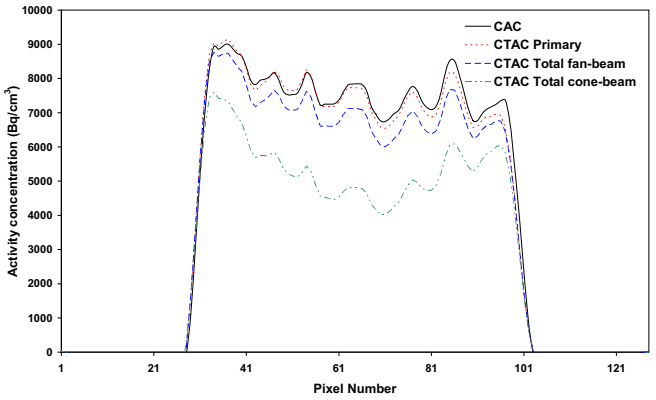

(b)

Fig. 3. (a) Reconstructed images of Monte Carlo simulated emission data corrected for attenuation using from left to right: CAC, CTAC primary, CTAC total fan-beam and CTAC total cone-beam. (b) Central profile through images shown in (a).

IV. Discussion

PET/CT now has emerged as an important and cost-effective method of performing anatomical-functional correlations in a way that improves patient management. The adoption of this technology has been rapid, and it is anticipated that the next phase of PET/CT likely will combine 3-D PET with volumetric cone-beam CT. This study revealed that the contamination of CT data with scattered radiation could generate some additional uncertainties during quantitative analysis of PET images when using CTAC if the CT images are not corrected for scatter [11]. The magnitude of propagated errors resulting from contribution of scatter in CT images depends on the object size and its chemical composition and more importantly on the geometry of the CT scanner. The scatter component in the next generation of cone-beam CT scanners based on flat panel detector geometry is significant and should be addressed to keep technology moving forward.

The bell shape of the scatter profile at 511 keV (Fig. 1) is due to the fact that the dominant interaction in this energy is Compton forward scattering. The higher value in the centre of the profile is the consequence of increased probability of Compton scattering with increasing the attenuation length in the central area of the cylindrical water phantom. The two peaks visible on the scatter profile at CT energy are the result of increasing the transmission probability of scattered photons with decreasing the attenuation length on the edges of the water phantom. It is worth to emphasize that the lower number of scattered photons in the centre of the profile for the CT energy is the result of either photoelectric absorption of incoming photons before undergoing Compton scattering or their absorption after Compton scattering. Although the amplitude of the scatter profile for 511 keV is higher, the acceptance of scattered photons in conventional radionuclide transmission scanning can be minimized by setting an appropriate energy discrimination window to reject scattered photons [12].

The underestimation of attenuation profiles for the cone-beam geometry is due to the high contamination of projection data with scattered radiation (Fig. 2). The magnitude of this contamination is rather small for the fan-beam geometry owing to the fact that scattered photons are either absorbed in septa plates placed between the detector elements or do not hit the detector elements because of limited detector's aperture in the *z*-axis (4 cm in multi-slice scanners). The underestimation of attenuation profiles reduces CT numbers in the central area of reconstructed images and creates cupping artefacts. Consequently, cupping artefacts in CT images will result in the underestimation of linear attenuation coefficients in the central area of μmaps generated using CTAC and thus the ACFs to be used for attenuation correction of the emission data. The underestimation of ACFs will induce underestimation of activity concentration in the central area of PET images (Fig. 3). In this study, the magnitude of the scatter component in both commercial multi-slice and prototype flat panel detector geometries was assessed [13]. Moreover, the contribution of scattered radiation during CTAC of PET images was quantified and used to identify correction strategies for better management of deleterious scatter effect, especially for the new generation of flat panel detector-based cone-beam CT scanners that may be combined with future generation panel-based PET scanners [6] to bring in a new design for large axial field-of-view PET/CT.

V. Conclusion

The impact of x-ray scatter on the accuracy of CT-based attenuation correction in PET was studied using Monte Carlo simulation. The contribution of x-ray scatter during the CTAC procedure was quantified for commercially available multi-slice CT and prototype large area flat panel detector-based cone-beam CT scanners. The magnitude of scatter in CT images for the cone-beam geometry is significant and might create cupping artifacts in reconstructed PET images during CTAC; however, its effect is small for current generation multi-slice fan-beam CT scanners using septa between detector elements, but should preferably be corrected during CT reconstruction to avoid quantification bias. These results substantiate the important role of antiscatter collimation and robust scatter correction algorithms which certainly will be

implemented in future generation flat panel based PET/CT scanners when used for quantitative measurements.

REFERENCES

[1] A. P. Colijn and F. J. Beekman, "Accelerated simulation of cone beam X-ray scatter projections.," *IEEE Trans. Med. Imaging*, vol. 23, pp. 584-590, 2004.

[2] J. H. Siewerdsen and D. A. Jaffray, "Cone-beam computed tomography with flat-panel imager: Magnitude and effects of x-ray scatter," *Med. Phys.*, vol. 28, pp. 220-231, 2001.

[3] M. R. Ay and H. Zaidi, "Development and validation of MCNP4C-based Monte Carlo simulator for fan- and cone-beam x-ray CT.," *Phys. Med. Biol.*, vol. 50, pp. 4863-4885, 2005.

[4] H. Zaidi, A. H. Scheurer, and C. Morel, "An object-oriented Monte Carlo simulator for 3D cylindrical positron tomographs," *Comput. Methods Programs Biomed.*, vol. 58, pp. 133-145, 1999.

[5] R. Ning and X. Tang, "X-ray scatter correction algorithm for cone beam CT imaging," *Med. Phys.*, vol. 31, pp. 1195-1202, 2004.

[6] D. W. Townsend, J. P. J. Carney, J. T. Yap, and N. C. Hall, "PET/CT today and tomorrow," *J Nucl Med*, vol. 45, pp. 4s-14s, 2004.

[7] M. Ay, M. Shahriari, S. Sarkar, M. Adib, and H. Zaidi, "Monte Carlo simulation of x-ray spectra in diagnostic radiology and mammography using MCNP4C.," *Phys. Med. Biol.*, vol. 49, pp. 4897-4917, 2004.

[8] H. Zaidi, "Comparative evaluation of scatter correction techniques in 3D positron emission tomography.," *Eur J Nucl Med*, vol. 27, pp. 1813-1826, 2000.

[9] H. Kanamori, N. Nakamori, K. Inoue, and E. Takenaka, "Effect of scattered x-ray on CT images," *Phys. Med. Biol.*, vol. 30, pp. 239-249, 1985.

[10] C. Bai, L. Shao, A. J. Da Silva, and Z. Zhao, "A generalized model for the conversion from CT numbers to linear attenuation coefficients.," *IEEE Trans Nucl Sci*, vol. 50, pp. 1510-1515, 2003.

[11] H. Zaidi and K. F. Koral, "Satter modelling and compensation in emission tomography," *Eur J Nucl Med*, vol. 31, pp. 761-782, 2004.

[12] M. Dahlbom and E. Hoffman, "Problems in signal-to-noise ratio for attenuation correction in high resolution PET," *IEEE Trans. Nucl. Sci.*, vol. 34, pp. 288-293, 1987.

[13] M. R. Ay and H. Zaidi, "Assessment of errors caused by x-ray scatter and use of contrast medium when using CT-based attenuation correction in PET.," *Eur J Nucl Med Mol Imaging*, vol. 33, 2006 *in press*